Identification of the Mott Insulating Charge Density Wave State in 1T-TaS$_2$

Dongbin Shin[1], Nicolas Tancogne-Dejean[1], Jin Zhang[1], Mahmut Sait Okyay[2]
Angel Rubio[1,3,4,*] and Noejung Park[2,†]

[1]*Max Planck Institute for the Structure and Dynamics of Matter and Center for Free-Electron Laser Science,*
Luruper Chaussee 149, 22761 Hamburg, Germany
[2]*Department of Physics, Ulsan National Institute of Science and Technology (UNIST), UNIST-gil 50, Ulsan 44919, Korea*
[3]*Nano-Bio Spectroscopy Group, Departamento de Fsica de Materiales, Universidad del Pas Vasco, 20018 San Sebastian, Spain*
[4]*Center for Computational Quantum Physics (CCQ), The Flatiron Institute, 162 Fifth Avenue, New York, New York 10010, USA*

We investigate the low-temperature charge density wave (CDW) state of bulk TaS$_2$ with a fully self-consistent density-functional theory with the Hubbard U potential, over which the controversy has remained unresolved regarding the out-of-plane metallic band. By examining the innate structure of the Hubbard U potential, we reveal that the conventional use of atomic-orbital basis could seriously misevaluate the electron correlation in the CDW state. By adopting a generalized basis, covering the whole David star, we successfully reproduce the Mott insulating nature with the layer-by-layer antiferromagnetic order. Similar consideration should be applied for description of the electron correlation in molecular solid.

A first-principle description of interacting many-body states has been a central issue in many areas of solid-state theories. While the density-functional theory (DFT) provides a formal route for finding the ground-state energy of a many-electrons system, the self-consistent density seeking procedure, as formulated by Kohn and Sham (KS), has been usually practiced with approximated local or semilocal functionals [1–6]. Those practical functionals lack the derivative discontinuity in the energy density functional [7–9] and usually underestimate the fundamental band gap and overestimate charge transfer [10–12]. Among various complementation schemes [3,13], the KS scheme combined with the Hubbard U potential, now known as DFT + U, has been most widely used particularly in the descriptions of the correlation-dominated insulating nature of the Mott insulating state [14–18]. On the other hand, when the on-site potential is not fully repulsive, as in cases of various bad-metal phases, the statistical samplings of multiple occupations are essentially required, as treated in the framework of the dynamical mean-field theory (DMFT) [19,20].

A four-decades-long debate has remained unresolved for the low-temperature phase of bulk TaS$_2$. Whereas many experiments reported the insulating charge density wave (CDW) phase [21–28], first-principle calculations with DFT and DFT + U have noticed that the in-plane Mott states constitute the metallic band dispersion along the out-of-plane direction [29–32]. It has experimentally reported that, on the formation of the low-temperature Mott insulating phase of the commensurate CDW phase at $T < 200$ K, the atomic structures are reconstructed into the David star pattern, packed in the $\sqrt{13} \times \sqrt{13}$ in-plane superlattice [24–28]. The Mott insulating nature of the monolayer has

been described with the first-principle calculations, and also the corresponding the two-dimensional (2D) Hubbard model Hamiltonian has been evaluated in the framework of DMFT [33–35]. However, on stacking of the 2D Mott insulating layers in the bulk 1T-TaS$_2$, the calculation results with DFT, DFT + U, and spin-frozen hybrid functional lose the separation between the lower Hubbard and upper Hubbard bands, resulting in a spin-unpolarized metallic dispersion along the out-of-plane direction [29–32]. These theoretical results clearly contrast with the experimentally observed insulating nature [21–28]. Leaving behind these inconsistencies, a variety of interests have been gathered on complex phase diagrams of TaS$_2$ [24,25]. Also, controllable phase transitions have been pursued to utilize the phase diagram as a memory device [26,36–39].

To resolve the inconsistency between the previous experiments and theories for the bulk 1T-TaS$_2$, here we reexamine the innate structure of the DFT + U [29–31]. In the standard formulation of the DFT + U, the total energy is expressed as a functional of both the electron density and the density matrix constructed in the correlated subspace $E_{\text{DFT}+U} = E_{\text{DFT}}[\rho(\mathbf{r})] + E_U[n]$ [14–16]. The averaged two-body energy is separated into the on-site Coulomb (U) and exchange energy (J), and by subtracting the doubly counted mean-field energy from the DFT energy functional, the effective Hubbard U energy can be expressed in terms of $\bar{U} = U - J$, as follows:

$$E_U = \sum_I \frac{\bar{U}_I}{2} \sum_{m,m',\sigma} \{n_{m,m'}^{I,\sigma}\delta_{m,m'} - n_{m,m'}^{I,\sigma}n_{m',m}^{I,\sigma}\}, \quad (1)$$

where $n^{I,\sigma}_{m,m'} = \sum_{i,\mathbf{k},\sigma} (1/N_{\mathbf{k}}) \langle \psi^{\sigma}_{i,\mathbf{k}} | \hat{P}^{I}_{m,m'} | \psi^{\sigma}_{i,\mathbf{k}} \rangle$, and $\hat{P}^{I}_{m,m'} = |\phi^{I}_{m}\rangle\langle\phi^{I}_{m'}|$. Above, $\psi^{\sigma}_{i,\mathbf{k}}$ indicates the KS orbital for the ith band with the Bloch vector $\mathbf{k}$ and spin state σ. ϕ^{I}_{m} represents the atomic-orbital basis, for the mth orbital of the Ith atom. $N_{\mathbf{k}}$ indicates the number of sampled $\mathbf{k}$ points in the Brillouin zone. The functional variation $\delta E_{\text{DFT}+U}/\delta\psi^{\sigma}_{i,\mathbf{k}}$ leads to one-body potential that depends on the electron density of the band states and the density matrix of the projected subspace [14–16].

Now we examine the characteristics of the functional with a simple molecular example. For a diatomic molecular orbital consisting of two one-orbital atoms, the Hubbard energy can be written as $E_{U} = \sum_{\sigma}(\bar{U}/2)[(n_{b\sigma} - n^{2}_{b\sigma}) + (n_{a\sigma} - n^{2}_{a\sigma})]$, where $n_{b\sigma}$ and $n_{a\sigma}$ represent the occupation numbers of the bonding and antibonding molecular orbitals with the spin state σ, respectively [40–42]. The sequence of electron occupations is schematically depicted in Fig. 1(a), assuming that the energy splitting between the bonding and antibonding states is substantially larger than the on-site interaction energy ($\bar{U}$). The sharp kinks in the plot of E_{U} in terms of electron numbers, as shown by the solid line in Fig. 1(b), illustrate clearly the well-known derivative discontinuity of the exact exchange-correlation functional at the integer numbers of particles [7–9].

One may consider the same system by counting the occupations of each atomic orbital. The Hubbard energy becomes $E^{\text{atom}}_{U} = \sum_{\sigma}(\bar{U}/2)[(n_{1\sigma} - n^{2}_{1\sigma}) + (n_{2\sigma} - n^{2}_{2\sigma})]$, with $n_{1\sigma}$ and $n_{2\sigma}$ indicating the occupation of the first and second atomic orbital with the spin (σ), respectively. Once the series of the electron occupation, shown in Fig. 1(a), is subject to the molecular symmetry, it is natural to claim that the two expressions of the density matrix are related by $n_{1\sigma} = n_{2\sigma} = \frac{1}{2}(n_{b\sigma} + n_{a\sigma})$. As revealed by the dashed red line in Fig. 1(b), the plot of the E^{atom}_{U} in terms of the electron number largely misses the kink structure at the point of the integer number of electrons [8,16]. This result indicates that the application of the Hubbard U potential onto each constituent atomic orbital is irrelevant, substantially misevaluating the electron correlation in molecular-orbital states.

To demonstrate this misbehavior in a more realistic example, we consider the O_2 molecule on the surface of a Cu(100) surface: O_2 molecule fixed to a distance of 5 Å above the three-layer Cu slab, as depicted in the inset of Fig. 1(c). The density of state of the O_2/Cu(100) system reveals the spin-triplet O_2 molecular state over the background metallic states of the Cu layer, as indicated by two pairs of arrows in Fig. 1(c). We added additional electrons to this system, and we calculated each ground state with the given number of electrons; the Bader charge is evaluated to account for the number of electrons accommodated in O_2, as shown in Fig. 1(d). When we calculated the system by using the Perdew-Burke-Ernzerhof (PBE)-type functional [6], these added electrons are fractionally distributed between O_2 and the metal layer, as shown in Fig. 1(d). We now consider applying the U potential onto generalized basis, hereafter abbreviated as DFT + GOU, and it is applied on O_2 molecular orbital states for this example. The resulting number of electrons in O_2 exhibit a sharp steplike increase, which proves the discontinuous jump in the Coulomb energy of the electrons occupying the O_2 rather than long-range partial charge transfer. Notably, the various U parameters in the conventional scheme resulted in similar fractional distributions, which clearly evidences our arguments on the misbehavior of the U applied onto the atomic orbitals.

In general, the U parameters are manually selected so as to reproduce the known electronic structure. However, a few recent approaches have proposed schemes to determine the on-site Coulomb (U) and exchange (J) parameters in a self-consistent way [16–18,43–46]. One well-known method was suggested by Agapito et al. (ACBN0) [17], in which the U and J parameters are determined through the theory of screened Hartree-Fock exchange potential in the correlated subspace [17,18,47]. In our study, hereafter, the Coulomb parameter calculated by this self-consistent ACBN0 scheme is denoted by $\bar{U}$, while the manually selected one is noted by U. For example, the computed parameter for O_2 molecular orbital in the O_2/Cu(100) system is found to be $\bar{U} \approx 7.5$ eV. Key elements of the formulations of the DFT + GOU (ACBN0) are summarized and the revival of the derivative discontinuity are discussed in the Supplemental Material [48].
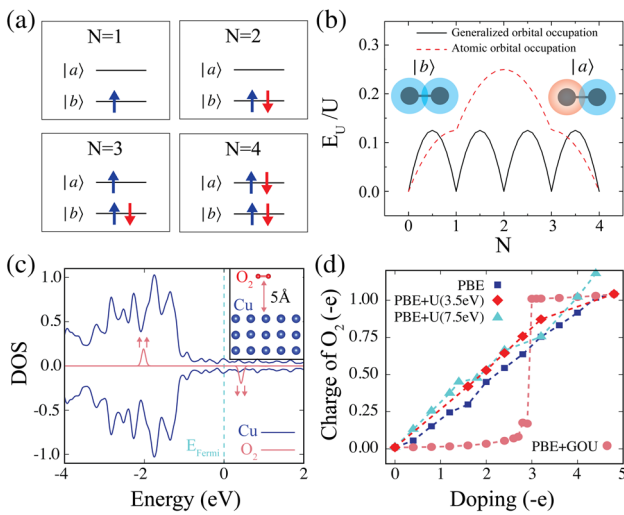

FIG. 1. (a) Various occupations of the molecular orbitals of the model diatomic molecule. (b) The Hubbard energy with respect to the electron number (N) as defined in (a). (c) Density of state for the O_2/Cu(100) system. (d) The charge of O_2 with respect to additional electron doping on the O_2/Cu(100) system. (a),(b) $|a\rangle$ and $|b\rangle$ indicate the bonding and antibonding molecular orbitals, respectively. Inset of (c) indicates schematic geometry of O_2 on Cu(100) surface. In (c), up- and downward arrows indicate doubly degenerated spin-up and spin-down states of O_2.
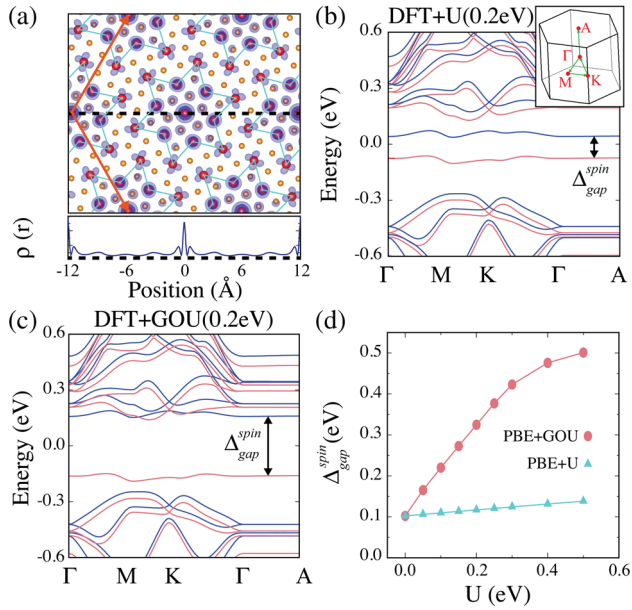
FIG. 2. (a) An isosurface of the valence band maximum CDW state overlapped on the atomic geometry of the monolayer 1T-TaS$_2$ (upper), and the same charge density on the line that passes through the central Ta atom of the star of David (lower). Band structure of monolayer 1T-TaS$_2$ calculated by (b) DFT+U ($U = 0.2$ eV) and (c) DFT + GOU ($U = 0.2$ eV). (d) The energy gap of monolayer 1T-TaS$_2$ with various Hubbard U values. Two arrows in orange in the upper panel of (a) indicate the lattice vector of the $\sqrt{13} \times \sqrt{13}$ supercell. The lattice length is $a = 12.13$ Å. The line for the charge density plot is depicted by the thick dashed line in both parts of (a). The red and orange balls indicate Ta and S atoms, respectively. The blue surface is the isosurface of partial charge density of CDW state. Cyan solid lines are the guide to the eye for David star pattern of the CDW. (b),(c) Red and blue solid lines indicate spin-up and spin-down states, respectively. The inset of (b) indicates the Bouillon zone of $\sqrt{13} \times \sqrt{13}$ supercell with high symmetric points.

The aforementioned scheme is well suited for the CDW state of the bulk 1T-TaS$_2$. Figure 2(a) depicts the commensurate CDW state of the David star pattern in the $\sqrt{13} \times \sqrt{13}$ supercell. The lobe of charge density indicates that the CDW state mainly consists of $5d_z$ orbitals of the Ta atoms at the center and six surrounding the vertex of the David star, which is also confirmed by the cross-sectional profile displayed in the lower panel of Fig. 2(a). The band structures of the monolayer calculated by DFT + U and DFT + GOU are displayed in Figs. 2(b) and 2(c), respectively, in which the flat band state below and above the Fermi level correspond to the singly occupied and unoccupied CDW states, respectively. For the generalized orbital to which the U potential is applied, we set the KS orbitals of the CDW state. Detailed procedures to derive the generalized basis orbital from the self-consistently converged Kohn-Sham states are summarized in the Supplemental Material [48]. The energy gap between the

spin-up valence band and spin-down conduction band are summarized in Fig. 2(d). The splitting between the upper and the lower Hubbard bands with respect to various U parameters obviously reveals the difference. The energy gap calculated by the DFT + GOU increases linearly with the U parameter, while the spin gap size in the DFT + U is mostly inert over the increase of the U parameter. Note that the difference in the Hubbard potential energy between occupied ($n_{CDW} = 1$) and unoccupied CDW states ($n_{CDW} = 0$) is exactly U, which can be read from $\hat{V}_U = (1/N_k) \sum_{\sigma,\mathbf{k}} U(\frac{1}{2} - n_{CDW,\sigma}) |\phi_{CDW,\sigma,\mathbf{k}}\rangle \langle \phi_{CDW,\sigma,\mathbf{k}}|$.

Now we focus on the band structure of bulk 1T-TaS$_2$, of which the out-of-plane conductivity has remained controversial for the last decade. In our study, we chose the A-stacked bulk 1T-TaS$_2$ as a representative example, in which the Ta center atom of the David star is on the top of the same atom in the adjacent layer [29–31,49]. We doubled the computational supercell to include two TaS$_2$ layers to investigate the layer-by-layer spin order. The band structure of the bulk 1T-TaS$_2$ calculated by the DFT exhibits a metallic band with a wide band width ($\sim$0.35 eV) along the out-plane direction (Γ-A), as shown in Fig. 3(a). Furthermore, as depicted in the upper panel of Fig. 3(a), this metallic band does not produce the spin splitting, and the spin-up and spin-down charge densities exhibit almost the same pattern.

On the other hand, the DFT + GOU scheme reveals a Mott insulating phase of the bulk 1T-TaS$_2$. In this study, the Hubbard U parameter is self-consistently determined by using the ACBN0 method ($\bar{U} = 0.33$ eV), which produces a sizable gap opening: the energy gap at the zone boundary A point (Δ_A) is 0.16 eV and the indirect band gap ($\Delta_{indirect}$) is 0.06 eV, which is the eigenvalues difference between the valence band maximum state at the A point and conduction band minimum state at the point of 20% along the path G–K. The experimental observed Mott gap ($\sim$0.12 eV) is comparable with our computed values [27]. The CDW band exhibits clear spin splittings, and the spin-up and spin-down band edges reside in different layers, as depicted by the partial charge densities of the CDW states shown in the upper panel of Fig. 3(b): the spin-down band in the first layer and the spin-up band in the next layer are denoted by the two numbered arrows. As a result, we obtained the layer-by-layer antiferromagnetic Mott insulating phase for the ground state of 1T-TaS$_2$.

For the comparison with experimental observations, we calculated the unfolded band structure into the primitive cell of 1T-TaS$_2$ using the BandUP code [50]. As shown in Figs. 3(c) and 3(d), the main difference between DFT and DFT + GOU methods can be found along the $\bar{\Gamma}$-$\bar{A}$ line. The unfolded band structure evaluated by the DFT + GOU (ACBN0) exhibits an apparent gap, which is in good agreement with recent angle-resolved photoemission spectroscopy measurement in the $\bar{\Gamma}$-$\bar{A}$ line [31,51]. For comparison, we tested with various U parameters, and the
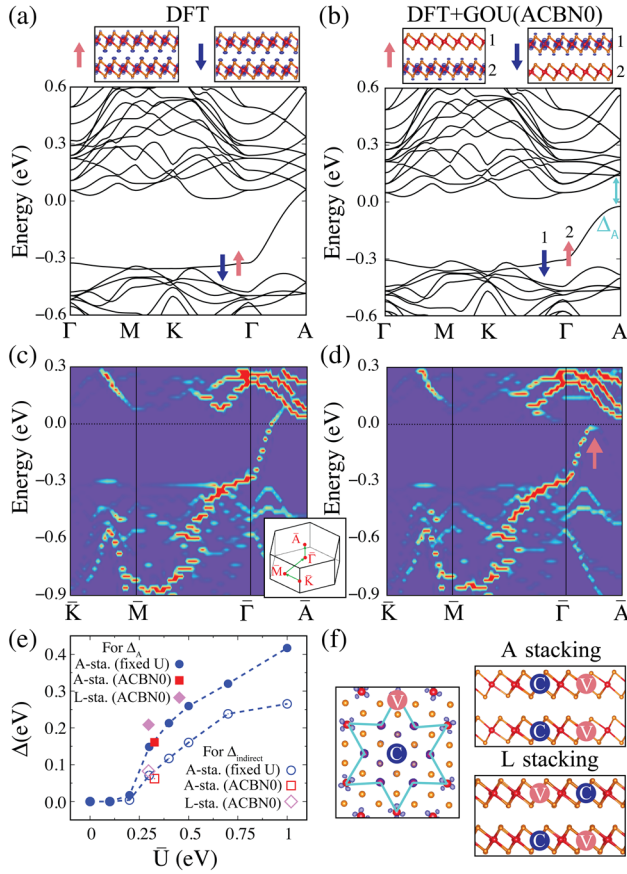
FIG. 3. Band structure of the bulk 1T-TaS$_2$ calculated by (a) DFT and (b) DFT $+$ GOU (ACBN0) methods. Unfolded band structure of bulk 1T-TaS$_2$ in the primitive cell calculated by (c) DFT and (d) DFT $+$ GOU (ACBN0) methods. (e) The gap at zone boundary (A) and the indirect band gap of the bulk 1T-TaS$_2$ with respect to the various values of the U parameters. (f) Schematic atomic geometry for A stacking and L stacking of the bulk 1T-TaS$_2$. In (a) and (b), the red and pink arrows indicate the spin-up and spin-down CDW states, respectively. Upper panels of (a) and (b) indicate partial charge density of CDW state for spin-up (left) and spin-down (right) at zone boundary (the A point). The two adjacent layers are denoted by 1 and 2. The inset of (c) indicates the Bouillon zone of primitive cell with high symmetric points.

obtained energy gaps are summarized in Fig. 3(e): the gaps at the zone boundary at the A point (Δ_A) and the band gap indirectly formed at different **k** points (Δ_{indirect}) are displayed with solid and empty symbols, respectively.

Now we consider different stacking orders and show that the obtained Mott insulating nature, in the result of DFT $+$ GOU, is independent of the stacking order. The center and vertex Ta atom of the David star are denoted as C and V sites, respectively, as shown in the left panel of Fig. 3(f). In the A-stacking geometry, the center Ta atoms (C site) is exactly on top of the same C site in the adjacent layer, as depicted in the right upper panel of Fig. 3(f). In the L-stacking geometry, the C site of one layer is on top of the

V site of the other layer, as shown in the right bottom panel of Fig. 3(f). In our self-consistent DFT $+$ GOU calculations with the ACBN0 functional, as summarized in Fig. 3(e), both the L-stacked and A-stacked bulk phases exhibit a similar size of the band gap.

Numerous experimental studies have investigated the conductivity changes near the phase boundary of the bulk TaS$_2$ [21–28]. Near the phase transition ($T \sim 200$ K), not only the in-plane conductivity but also the out-of-plane conductivity changes drastically [28]. Measurements and discussions on the spin configurations are diverse [28,33,34,52], but the insulating nature of the bulk TaS$_2$ is experimentally agreed [21–24,28]. A recent first-principle calculation suggested that a very particular double-layer stacking order leads to a band gap without spin ordering [31,53]. On the other hand, recent scanning tunneling microscopy and transmission electron microscopy revealed that the Ta atoms in different layers are in good order along the out-of-plane direction [49], and such type of double-layer order is not likely in practice [54]. Our results of the DFT $+$ GOU, as summarized in Fig. 3(e), indicates that the bulk preserves the Mott insulating phase irrespective of the stacking order, which supports all the experimental results mentioned above and suggest that the 3D insulating nature should obviously be attributed to the Coulomb correlation in the David star.

In summary, we reinvestigated the Mott insulating nature of bulk 1T-TaS$_2$ whose electronic structure evaluated by DFT provides inconsistent results from previous experimental observations. We showed that the conventional Hubbard U potential can lead to erroneous evaluation of the electron correlation in KS states rooted in multiple atoms [55]. By applying DFT $+$ GOU, we successfully reproduced the Mott insulating phases of the bulk 1T-TaS$_2$ with the layer-by-layer antiferromagnetic order, which resolves the decades-long inconsistency that has occurred by DFT calculation. The electron correlation in orbitals localized, but extended over atoms, should be considered with similar perspective.

Computational details.—We performed DFT calculation using the Quantum ESPRESSO package [56] with PBE-type functional [6]. The projector-augmented wave method is used, and the plane wave basis set with 30 and 60 Ry energy cutoff is used to describe wave function for 1T-TaS$_2$ and O$_2$/Cu(100) systems, respectively. The calculated lattice constant for bulk 1T-TaS$_2$ is $a = 3.36$ Å and $c = 5.9$ Å [57]. The Brillouin zone is sampled with $5 \times 5 \times 10$ **k**-point mesh for 1T-TaS$_2$ systems, and the $8 \times 8 \times 1$ **k**-point sampling is used for the O$_2$/Cu(100) system.

---

*angel.rubio@mpsd.mpg.de
†noejung@unist.ac.kr

[1] J. P. Perdew and M. Levy, Phys. Rev. Lett. **51**, 1884 (1983).

[2] W. Kohn and L. J. Sham, Phys. Rev. **140**, A1133 (1965).

[3] J. P. Perdew and A. Zunger, Phys. Rev. B **23**, 5048 (1981).

[4] D. M. Ceperley and B. J. Alder, Phys. Rev. Lett. **45**, 566 (1980).

[5] J. P. Perdew, K. Burke, and M. Ernzerhof, Phys. Rev. Lett. **77**, 3865 (1996).

[6] J. P. Perdew and Y. Wang, Phys. Rev. B **45**, 13244 (1992).

[7] J. F. Janak, Phys. Rev. B **18**, 7165 (1978).

[8] X. Andrade and A. Aspuru-Guzik, Phys. Rev. Lett. **107**, 183002 (2011).

[9] J. D. Chai and P. T. Chen, Phys. Rev. Lett. **110**, 033002 (2013).

[10] V. I. Anisimov, J. Zaanen, and O. K. Andersen, Phys. Rev. B **44**, 943 (1991).

[11] D. Shin, G. Lee, Y. Miyamoto, and N. Park, J. Chem. Theory Comput. **12**, 201 (2016).

[12] D. Shin, H. Jung, S. S. Han, C. H. Choi, H. Lee, and N. Park, Chem. Phys. Lett. **570**, 85 (2013).

[13] J. Heyd, G. E. Scuseria, and M. Ernzerhof, J. Chem. Phys. **118**, 8207 (2003).

[14] V. I. Anisimov, I. V. Solovyev, M. A. Korotin, M. T. Czyżyk, and G. A. Sawatzky, Phys. Rev. B **48**, 16929 (1993).

[15] A. I. Liechtenstein, V. I. Anisimov, and J. Zaanen, Phys. Rev. B **52**, R5467(R) (1995).

[16] M. Cococcioni and S. de Gironcoli, Phys. Rev. B **71**, 035105 (2005).

[17] L. A. Agapito, S. Curtarolo, and M. Buongiorno Nardelli, Phys. Rev. X **5**, 011006 (2015).

[18] N. Tancogne-Dejean, M. A. Sentef, and A. Rubio, Phys. Rev. Lett. **121**, 097402 (2018).

[19] A. Georges, G. Kotliar, W. Krauth, and M. J. Rozenberg, Rev. Mod. Phys. **68**, 13 (1996).

[20] G. Kotliar and D. Vollhardt, Phys. Today **57**, No. 3, 53 (2004).

[21] J. A. Wilson, F. J. Di Salvo, and S. Mahajan, Adv. Phys. **24**, 117 (1975).

[22] P. Fazekas and E. Tosatti, Physica (Amsterdam) **99B+C**, 183 (1980).

[23] B. Dardel, M. Grioni, D. Malterre, P. Weibel, Y. Baer, and F. Lévy, Phys. Rev. B **45**, 1462 (1992).

[24] B. Sipos, A. F. Kusmartseva, A. Akrap, H. Berger, L. Forró, and E. Tut, Nat. Mater. **7**, 960 (2008).

[25] T. R. T. Han, F. Zhou, C. D. Malliakas, P. M. Duxbury, S. D. Mahanti, M. G. Kanatzidis, and C. Y. Ruan, Sci. Adv. **1**, e1400173 (2015).

[26] S. Hellmann, M. Beye, C. Sohrt, T. Rohwer, F. Sorgenfrei, H. Redlin, M. Kalläne, M. Marczynski-Bühlow, F. Hennies, M. Bauer, A. Föhlisch, L. Kipp, W. Wurth, and K. Rossnagel, Phys. Rev. Lett. **105**, 187401 (2010).

[27] S. Hellmann, T. Rohwer, M. Kalläne, K. Hanff, C. Sohrt, A. Stange, A. Carr, M. M. Murnane, H. C. Kapteyn, L. Kipp, M. Bauer, and K. Rossnagel, Nat. Commun. **3**, 1069 (2012).

[28] E. Martino, A. Pisoni, L. Ćirić, A. Arakcheeva, H. Berger, A. Akrap, C. Putzke, P. J. Moll, I. Batistić, E. Tutiš, L. Forró, and K. Semeniuk, npj 2D Mater. Appl. **4**, 7 (2020).

[29] P. Darancet, A. J. Millis, and C. A. Marianetti, Phys. Rev. B **90**, 045134 (2014).

[30] T. Ritschel, J. Trinckauf, K. Koepernik, B. Büchner, M. V. Zimmermann, H. Berger, Y. I. Joe, P. Abbamonte, and J. Geck, Nat. Phys. **11**, 328 (2015).

[31] S. H. Lee, J. S. Goh, and D. Cho, Phys. Rev. Lett. **122**, 106404 (2019).

[32] P. Lazar, J. Martincova, and M. Otyepka, Phys. Rev. B **92**, 224104 (2015).

[33] L. Perfetti, T. A. Gloor, F. Mila, H. Berger, and M. Grioni, Phys. Rev. B **71**, 153101 (2005).

[34] L. Perfetti, P. A. Loukakos, M. Lisowski, U. Bovensiepen, H. Berger, S. Biermann, P. S. Cornaglia, A. Georges, and M. Wolf, Phys. Rev. Lett. **97**, 067402 (2006).

[35] T. Yoshioka, A. Koga, and N. Kawakami, Phys. Rev. Lett. **103**, 036401 (2009).

[36] I. Vaskivskyi, J. Gospodaric, S. Brazovskii, D. Svetin, P. Sutar, E. Goreshnik, I. A. Mihailovic, T. Mertelj, and D. Mihailovic, Sci. Adv. **1**, e1500168 (2015).

[37] M. Yoshida, T. Gokuden, R. Suzuki, M. Nakano, and Y. Iwasa, Phys. Rev. B **95**, 121405(R) (2017).

[38] Y. Yu, F. Yang, X. F. Lu, Y. J. Yan, Y. H. Cho, L. Ma, X. Niu, S. Kim, Y. W. Son, D. Feng, S. Li, S. W. Cheong, X. H. Chen, and Y. Zhang, Nat. Nanotechnol. **10**, 270 (2015).

[39] J. Zhang, C. Lian, M. Guan, W. Ma, H. Fu, H. Guo, and S. Meng, Nano Lett. **19**, 6027 (2019).

[40] P. J. Strebel and Z. G. Soos, J. Chem. Phys. **53**, 4077 (1970).

[41] S. Chittipeddi, K. R. Cromack, J. S. Miller, and A. J. Epstein, Phys. Rev. Lett. **58**, 2695 (1987).

[42] F. Lechermann, A. Georges, G. Kotliar, and O. Parcollet, Phys. Rev. B **76**, 155102 (2007).

[43] H. J. Kulik and N. Marzari, J. Chem. Phys. **134**, 094103 (2011).

[44] N. J. Mosey, P. Liao, and E. A. Carter, J. Chem. Phys. **129**, 014103 (2008).

[45] N. J. Mosey and E. A. Carter, Phys. Rev. B **76**, 155123 (2007).

[46] J. Spencer and A. Alavi, Phys. Rev. B **77**, 193110 (2008).

[47] N. Tancogne-Dejean and A. Rubio, Phys. Rev. B **102**, 155117 (2020).

[48] See Supplemental Material at http://link.aps.org/supplemental/10.1103/PhysRevLett.126.196406 for implementation of ACBN0 in DFT + GOU scheme, revival of derivative discontinuity, and generation of generalized orbital basis set, which includes Refs. [17, 44–46].

[49] R. Hovden, A. W. Tsen, P. Liu, B. H. Savitzky, I. El Baggari, Y. Liu, W. Lu, Y. Sun, P. Kim, A. N. Pasupathy, and L. F. Kourkoutis, Proc. Natl. Acad. Sci. U.S.A. **113**, 11420 (2016).

[50] P. V. C. Medeiros, S. S. Tsirkin, S. Stafström, and J. Björk, Phys. Rev. B **91**, 041116(R) (2015).

[51] A. S. Ngankeu, S. K. Mahatha, K. Guilloy, M. Bianchi, C. E. Sanders, K. Hanff, K. Rossnagel, J. A. Miwa, C. Breth Nielsen, M. Bremholm, and P. Hofmann, Phys. Rev. B **96**, 195147 (2017).

[52] K. T. Law and P. A. Lee, Proc. Natl. Acad. Sci. U.S.A. **114**, 6996 (2017).

[53] T. Ritschel, H. Berger, and J. Geck, Phys. Rev. B **98**, 195134 (2018).

[54] C. J. Butler, M. Yoshida, T. Hanaguri, and Y. Iwasa, Nat. Commun. **11**, 2477 (2020).

[55] L. Xian, D. M. Kennes, N. Tancogne-Dejean, M. Altarelli, and A. Rubio, Nano Lett. **19**, 4934 (2019).

[56] P. Giannozzi *et al.*, J. Phys. Condens. Matter **29**, 465901 (2017).

[57] F. L. Givens and G. E. Fredericks, J. Phys. Chem. Solids **38**, 1363 (1977).